

# Temperature-Dependent I/Q Imbalance Compensation in Ultra-Wideband Millimeter-Wave Multi-Gigabit Transmitters

Ainhoa Rezola<sup>ID</sup>, Juan F. Sevillano, *Senior Member, IEEE*, David del Río<sup>ID</sup>, *Member, IEEE*, Belén Martín, Iñaki Gurutzeaga, Igone Vélez, *Member, IEEE*, and Roc Berenguer, *Senior Member, IEEE*

**Abstract**—Changes in ambient temperature or chip temperature result in variations in the in-phase and quadrature (I/Q) gain and phase imbalance. As a consequence, the overall system performance can be seriously degraded, especially in wideband multi-Gb/s systems, where the I/Q imbalance is highly selective in frequency. Unless appropriately considered, temperature drifts can decrease the image rejection ratio (IRR) of the transmitter. This article presents a novel compensation method for temperature-dependent transmitter I/Q imbalance over the entire temperature range. It consists of a simple predistortion technique that, based on a few factory characterizations of gain and phase imbalance, is able to estimate and correct the I/Q imbalance at any temperature, without interrupting the normal functionality of the system. The proposed method is assessed in a 2-GHz, 64-QAM transceiver implemented with real hardware. The measurements show that the proposed approach is able to keep the IRR greater than 35 dB in the entire bandwidth and an error vector magnitude (EVM) lower than 3% over a temperature range of 70 °C.

**Index Terms**—Digital predistortion, in-phase and quadrature (I/Q) imbalance, millimeter-wave (mmW), temperature, ultra-wideband (UWB).

## I. INTRODUCTION

HIGH-SPEED communications over wideband wireless channels have emerged as a key feature of future communications' systems. The demand for more data has motivated the utilization of ultra-wideband (UWB) channels in order to provide the data rates required for future applications [1]. However, the implementation of wideband wireless systems needs to address some challenging issues. A limiting issue in the implementation of low-cost, low-power, and fully integrated wireless systems is the impairments associated with the analog chain due to component imperfections [2], [3].

Analog components cannot be made to achieve the desired performance due to limitations in technology, cost, power consumption, or chip areas and these imperfections can reduce

Manuscript received April 4, 2019; revised July 13, 2019; accepted August 19, 2019. Date of publication October 8, 2019; date of current version January 13, 2020. This work was supported by the European Community's Framework Programme FP7/2007-2013 under Grant 317957. Consortium: Ceit, FhG, ALU-I, CEA-Leti, INCIDE, SiR, ST-I, Sivers IMA, and OTE. (Corresponding author: Ainhoa Rezola.)

A. Rezola, B. Martín, and R. Berenguer are with the Electrical and Electronic Engineering Department, TECNUN—University of Navarra, 20018 San Sebastián, Spain (e-mail: argarcia@ceit.es).

J. F. Sevillano, D. del Río, I. Gurutzeaga, and I. Vélez are with the ICT Division, Ceit-IK4, 20018 San Sebastián, Spain.

Color versions of one or more of the figures in this article are available online at <http://ieeexplore.ieee.org>.

Digital Object Identifier 10.1109/TMTT.2019.2943335

the system performance. Moreover, when the carrier frequency is high (>10 GHz) and the bandwidth is ultrawide (>500 MHz), the analog impairments can dominate the system performance.

In order to compensate for these imperfections, an approach that has gained momentum is to accept the RF impairments up to a certain degree and to compensate them digitally. This enables keeping power consumption, size, and cost of the transceiver (TRx) at desirable low levels and takes advantage of advanced technology nodes with high levels of digital integration. That is why, in order to enhance performance and reduce costs, digital compensation has become a must in recent years [4].

One of the most prominent impairments that degrades the system performance of wideband systems is the in-phase and quadrature (I/Q) imbalance caused by gain and phase mismatches between the I and Q paths of the analog front end. This impairment reduces the image rejection ratio (IRR) and, ultimately, leads to a degradation of the overall performance of the TRx [5], [6]. The literature offers multiple approaches to compensate for transmitter I/Q imbalance in the analog domain [7]–[10]. These methods rely on integrated tuning knobs that modify the gain in the I/Q signal paths and the phase difference in the quadrature local oscillator (LO) distribution network in order to achieve IRR values in the order of 30–40 dB. However, these systems add complexity to the integrated circuits (ICs) and the wideband channels are usually not able to compensate for frequency-selective imbalances caused by external components in the baseband I and Q paths (VGAs, low-pass filters, connectors, and DACs). Hence, in recent years, digital compensation techniques using signal processing algorithms have become popular [2], [6], [11], [12]. One of the main advantages of these methods is that they can be potentially applied to any commercial off-the-shelf (COTS) transmitter, therefore not requiring costly and complex *ad hoc* IC design. The most common approach to digitally mitigate the I/Q imbalance is the predistortion. Predistortion means applying an algorithm to the baseband signal in the digital domain, in such a way that when the predistorted signal goes through the analog front end, the output RF signal is I/Q balanced. In order to digitally predistort the transmitted signal, the I/Q imbalance of the transmitter has to be estimated.

Depending on different system assumptions, such as the frequency selectivity, the waveform, or the communication standard, different approaches for I/Q imbalance estimation

have been reported [2], [5], [6], [11]–[14]. However, a very few of them investigate the effect of environmental changes, such as the device temperature or supply voltage variations. Reference [15] evaluates the sensitivity of different RF imperfections to the temperature and, after analyzing the carrier frequency offset (CFO), power amplifier (PA) nonlinearity, dc offsets, and I/Q gain and phase imbalance, this article concludes that the parameter that most clearly changes with temperature is the I/Q phase imbalance, which suffers from significant drifts with temperature.

Various techniques that allow to minimize process–voltage–temperature (PVT) variations of PAs have been published, offering compensation methods of PA performance over these variations [16]–[18]. With regard to I/Q imbalance compensation, only a few analog-domain methods are robust against PVT variations. The work in [7] can dynamically adjust the imbalance in the LO path when environmental conditions change without stopping the communication, but it is sensitive to frequency-selective amplitude and phase imbalance in the baseband components. As for DSP-based methods, although there are methods able to compensate for process variations, to the best of our knowledge, PVT-dependent I/Q imbalance digital compensation methods have not been proposed for wideband multi-Gb/s systems.

PVT variations can affect the performance of the device and consequently, degrade the signal-to-noise ratio (SNR). For instance, if the I/Q imbalance has been estimated at a different temperature than the temperature at which the system is being operational, its performance can be seriously deteriorated. Temperature drifts can degrade the achievable IRR and other figures of merit, such as SNR or error vector magnitude (EVM). In order to maintain these parameters at desirable levels, the temperature should be monitored and appropriate changes should be made to the I/Q imbalance compensation according to changes in the temperature [13], [19].

This article studies the influence of temperature variations over the I/Q imbalance and offers a novel technique to compensate for temperature-dependent transmitter frequency-selective I/Q imbalance for wideband multi-Gb/s transmitters. The method, which consists of a digital predistortion, is able to compensate for the I/Q imbalance without interrupting the normal functionality of the system. The rest of this article is structured as follows. Section II provides a description of the system architecture, putting special emphasis on the issue of I/Q imbalance. Section III describes the measurement setup and the measurement procedure. Section IV evaluates the impact of temperature variations on the presented system and Section V proposes different approaches to deal with the frequency-selective I/Q imbalance under the influence of the temperature. These techniques are validated and compared with each other using a real hardware setup. Finally, the main conclusions are drawn in Section VI.

## II. SYSTEM ARCHITECTURE AND IMPAIRMENTS

This article considers a zero-intermediate frequency (IF) quadrature upconversion system, which can be part of a direct-conversion transmitter or a double-conversion transmitter, in which the signal is first converted to an IF and then

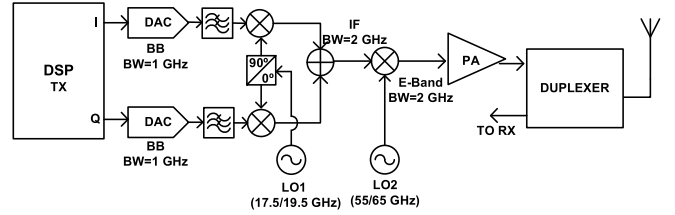


Fig. 1. Architecture of the transmitter of the point-to-point communication system.

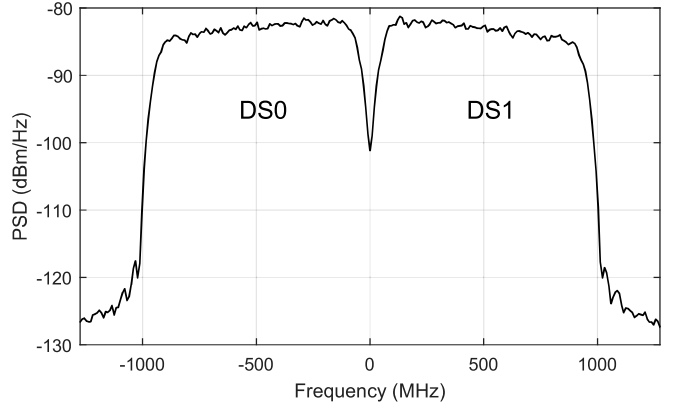


Fig. 2. Spectrum of the baseband signal with Hierarchical QAM modulation.

upconverted to a higher frequency band. The architecture of the latter is depicted in Fig. 1, which makes up a wideband mm-wave transmitter operating in the E-band like the one proposed in [20]. This system will be used for the analysis performed in this article, although the proposed method is potentially applicable to any other zero-IF upconverter. The system uses a 64-QAM modulation with a signal bandwidth of 2 GHz. The digital baseband processor (DSP-TX), implemented in a high performance FPGA, performs the coding, modulation, and pulse shaping of the bits to be transmitted. The digital samples of the modulated signal produced by the transmitter digital baseband are converted into analog signals in the DACs running at frequencies above 2 Gsp. The analog front end performs the required filtering before up-converting the baseband I and Q channels to an IF in the 15–21 GHz band. The IF signal is up-converted to the E-band by means of the millimeter-wave (mmW) mixer. Finally, the wideband mmW PA is in charge of amplifying the mmW signal to be transmitted. Due to the high channel bandwidth and high order modulation, this architecture presents some issues that should be addressed in order not to degrade the performance of the TRx. An important source of signal corruption is the ac coupling between different baseband components, which leads to a high pass filtering of the signal [21]. The approach taken to address this issue is to use a Hierarchical QAM modulation, where the outputs of two individual modulators are added in order to form the desired 2-GHz signal. The occupied baseband bandwidth of each sub-QAM is 1 GHz and, at the output of the Hierarchical QAM modulator, one sub-QAM (DS0) is centered at -500 MHz and the other sub-QAM (DS1) is centered at 500 MHz. By adding these two complex QAM modulated signals, the waveform shown in Fig. 2 is obtained, whose spectrum has a null at dc.

Yet, other imperfections such as the I/Q gain and phase imbalance have the potential to introduce a large degradation in the system performance, especially when high-order modulations are used [22]. Besides, when working with wideband systems, such as the one proposed in this article, the overall effective I/Q imbalance can vary as a function of the frequency over the whole band, contributing to further degradation. This impairment has been identified as the main source of degradation in the considered system [23].

In the literature there are several works addressing the transmitter I/Q imbalance compensation. In most cases, the I/Q imbalance estimation is done during regular operation of the system i.e., they do not require a dedicated calibration mode [14], [24]–[26]. These are usually blind techniques, meaning that the adaptation of the pre-compensation is done using only the knowledge of the statistics of the real information carrying signal. These techniques allow to perform a calibration of the device at periodic intervals without interrupting its normal operation, which enables estimating time-varying I/Q imbalance caused by temperature, biasing voltage and aging effects [27], [28].

While this kind of techniques offer the possibility to follow time-variant changes in the TRx front end, they present a major drawback when applied to the transmitter: the imbalance parameter estimation circuit includes a feedback loop from RF back to the transmitter digital baseband with an additional ADC, so as to sample the RF output. This is because, in order to digitally predistort the signal to compensate for the I/Q imbalance, the digital signal processor requires having some reference of the I/Q imbalance introduced by the analog front end. As the whole effective signal is transmitted for parameter estimation, a sampling rate of twice the signal bandwidth is required for this ADC. When dealing with wideband signals, as the 2 GHz considered in this article, it would lead to a very high sampling rate of the ADC (>4 Gs/s), which consumes several watts of power. Thus, such an approach is impractical for wideband systems.

So as to avoid the need for a high-speed ADC, a method based on spectral measurements using conventional laboratory equipment is presented in [29] and a BiSC approach is proposed in [6], both of them dealing with transmitter frequency-selective I/Q imbalance in the system proposed in this article. They consist of off-line calibration techniques that need to feed the transmitter with a series of digitally generated calibration signals and measure the resulting RF response. In contrast to [29], [6] consists of a novel approach, which does not require an expensive laboratory equipment for I/Q imbalance estimation. The measurement circuitry is integrated into the system to be calibrated rather than being outside, which enables in-field calibration in different operating conditions. Nonetheless, calibration requires interrupting data transmission. These techniques are not blind, meaning that they rely on special training signals and they need to interrupt the normal transmission to perform the calibration. Thus, in order to compensate for time-varying I/Q imbalance, these techniques would require to stop the transmission to perform a calibration from time to time.

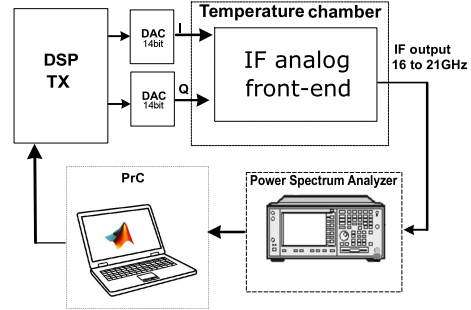


Fig. 3. Block diagram of temperature test setup.

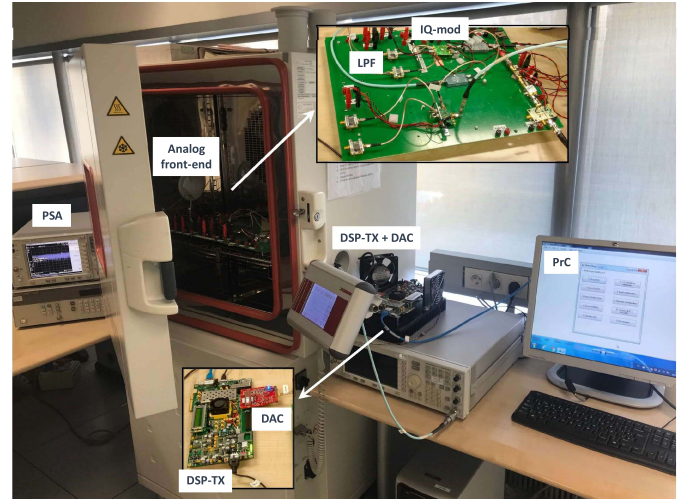


Fig. 4. Photograph of the measurements setup.

During normal operation of the transmitter, temperature will change. It is known that temperature drifts result in changes in the I/Q imbalance characteristics [19], [30]. If we are able to characterize the impact of temperature variations on the I/Q imbalance, it might be possible to derive an approach to compensate for the time-varying I/Q imbalance without the need to interrupt the data transmission.

### III. MEASUREMENT SETUP

In order to accurately characterize the I/Q imbalance of the system, temperature-dependent I/Q imbalance measurements have been performed in the aforementioned system. Fig. 3 shows a block diagram of the setup used to evaluate the temperature impact on I/Q imbalance and Fig. 4 shows a photograph of the measurement setup. The digital baseband processor (DSP-TX) is implemented in a Virtex-7 FPGA prototyping board (VC707) [31]. The FPGA is programmed in order to generate data bits and transform them into 64-QAM I/Q symbols. These symbols are pulse shaped by an RRC filter and a mixer modulates each digital subband to subcarriers at 500 and  $-500$  MHz, generating the waveform shown in Fig. 2. The final stage of digital baseband processing is the I/Q imbalance precompensation filter. The structure of this filter is shown in [6]. At the output of DSP-TX, a couple of high-speed DACs are responsible for converting the complex

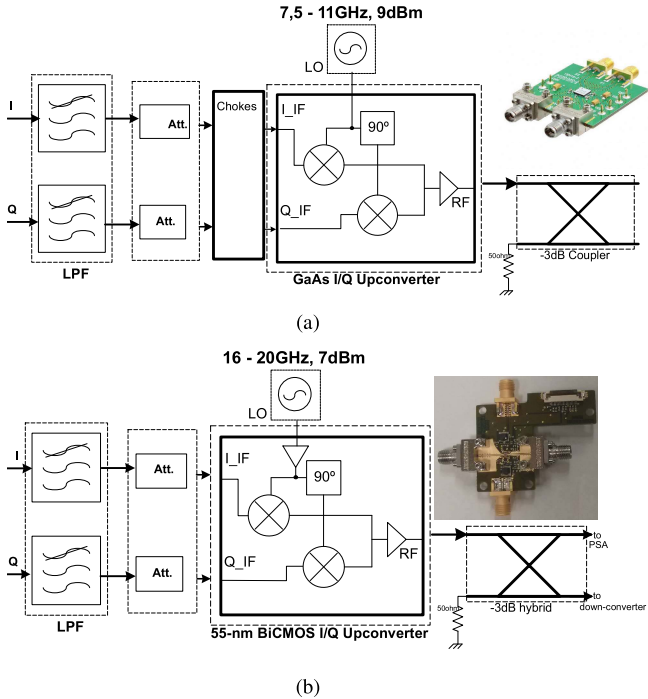


Fig. 5. Analog front ends. (a) Harmonic I/Q upconverter implemented in GaAs. (b) 55-nm SiGe BiCMOS I/Q upconverter.

baseband signal to the analog domain. The DAC board is a 4DSP FMC230 board, which contains a couple of 14-bit DACs working at 2.45 Gs/s [32].

Regarding the IF analog front end, two different front ends were analyzed in order to see whether the observed behavior of I/Q imbalance over temperature is repeatable or not. The block diagram of each front end is shown in Fig. 5, together with a picture of the upconverter boards. In both front ends, the I and Q channels coming from the DACs go through their corresponding low-pass filters (Mini Circuits LFCN-1000D) in order to filter the replicas produced by the DACs. The low-pass filters are followed by passive attenuators, which adjust the signal levels in the transmitter chain. In the first analog front end, at the output of the attenuators, a couple of chokes are placed in order to cancel the LO leakage and dc offset of the analog front end by applying proper dc voltages, as it is shown in Fig. 5(a). Following the chokes, a GaAs harmonic upconverter (Hittite HMC710LC5) is used to upconvert the signal. The LO signal goes through an internal active x2 multiplier. In the second analog front end, the output of the attenuators is directly connected to a 55-nm SiGe BiCMOS upconverter, as it is shown in Fig. 5(b). For this upconverter, an external buffer is used to amplify the LO signal. In both the cases, at the output of the I/Q upconverter, a  $-3\text{dB}$  hybrid is placed. This way, it is possible to see the upconverted spectrum at RF and, at the same time, feed a downconverter that brings the RF signal back to a low-IF for demodulation.

As shown in Figs. 3 and 5, not only the I/Q upconverter MMIC is introduced inside the temperature chamber but also the analog components in the I and Q branches (filters and attenuators). The cascade response of the I and Q branches

may not be identical and this mismatch will also contribute to I/Q imbalance. At the output of the I/Q modulator, once the I and Q signals have been added together after the first upconversion, no further I/Q imbalance will be introduced. Therefore, the E-band part of the architecture shown in Fig. 1 was not included in this article.

The output of the IF analog front end is connected to a power spectrum analyzer (PSA) in order to capture the transmitted signal and measure the power of certain test tones used to estimate the imbalance [23]. The information captured by the PSA is received by a prototype controller (PrC) implemented on a PC. Based on the collected data, a MATLAB software generates the appropriate control and configuration signals for DSP-TX during the calibration procedure to estimate the frequency-selective gain and phase imbalance. Moreover, this software calculates the actual coefficients of the I/Q imbalance precompensator filter and it can send them to DSP-TX. In order to perform the measurements, the desired temperature is programmed in the control panel of the temperature chamber. Once the temperature is stable in the chamber, the different measurements are started. The different procedures performed at each temperature are separated several minutes to ensure that the dynamics of the system are stable.

Once the temperature is stable, a measurement campaign can be started at that temperature. A full calibration is performed to estimate the current I/Q imbalance at this temperature. In order to obtain the results presented in this article, different sets of coefficients can be downloaded from PrC to DSP-TX to perform measurements.

In order to assess the achieved I/Q imbalance compensation, the IRR is measured using the transmission of tones and the PSA. Moreover, in order to assess the performance of the system, two types of measurements are performed. First, only one of the 1-GHz subbands is transmitted. The spectrum is monitored with a PSA to check if the images generated by the I/Q imbalance are properly removed. The same procedure is repeated for the other subband. Second, the whole 2-GHz signal is transmitted. The signal at the output of the I/Q modulator is downconverted to a low-IF of 1.25 GHz and captured using a high-speed digital oscilloscope. The captured signal is demodulated off-line using MATLAB to obtain the signal constellation and measure the modulation error ratio (MER) and EVM. The time between the measurements at the same temperature can be up to several minutes.

#### IV. TEMPERATURE IMPACT ON I/Q IMBALANCE

##### A. Measurement Results With GaAs MMIC Upconverter

Fig. 6 shows the measured I/Q phase ( $\phi_{tx}$ ) and gain ( $\alpha_{tx}$ ) imbalance over frequency when the upconverter implemented in GaAs was used. It is shown that the analog front-end I/Q imbalance is highly selective in frequency. The frequency band between 16.5 and 17.5 GHz presents higher gain and phase imbalance compared to the frequency band between 18 and 18.5 GHz.

Due to the I/Q imbalance, an undesired image component is generated at the mirror frequency of the desired signal. The most common figure of merit that characterizes the I/Q

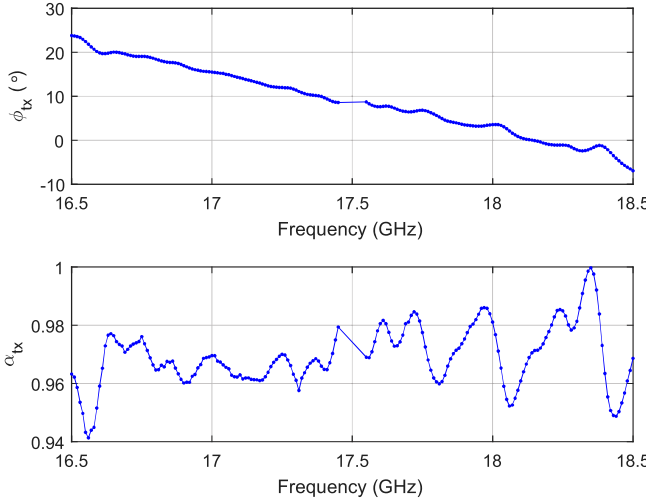


Fig. 6. I/Q gain and phase imbalance.

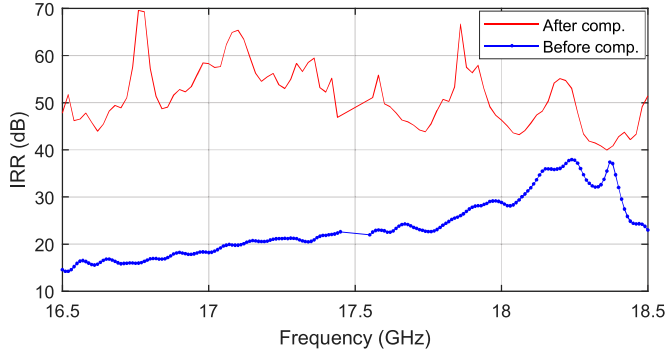


Fig. 7. IRR before and after compensation.

imbalance is the IRR. The IRR is the ratio between the signal level of the desired signal and the image signal. The curve labeled “Before comp.” of Fig. 7 shows the measured IRR of the analog front end. The IRR is lower in the frequency range between 16.5 and 17.5 GHz due to higher phase mismatches in this frequency band. The curve labeled “After comp.” represents the IRR after the I/Q imbalance has been compensated using one of the methods presented in [6].

Fig. 8 shows the measured I/Q gain and phase imbalance curves for different temperatures relative to the gain and phase imbalance curves measured at 25 °C. For example, the curves labeled “10 °C” are defined as

$$\Delta\phi_{tx10^\circ} = \phi_{tx10^\circ}(f) - \phi_{tx25^\circ}(f) \quad (1)$$

$$\Delta\alpha_{tx10^\circ} = \alpha_{tx10^\circ}(f) - \alpha_{tx25^\circ}(f). \quad (2)$$

According to this definition, the curve at 25 °C should be zero. In the gain imbalance curves,  $\Delta\alpha_{tx}$ , the variations with temperature are not very considerable. However, if we analyze the phase imbalance curves,  $\Delta\phi_{tx}$ , we can observe phase differences up to 2° when the temperature is at 70 °C. Analyzing Fig. 8, we can appreciate that the gain and phase imbalance curves are shifted with temperature. Fig. 9 shows the impact on the IRR when a factory calibration of I/Q imbalance has been performed at ambient temperature (25 °C) and the system is working at a different temperature (70 °C). The figure also compares the IRR when the calibration was

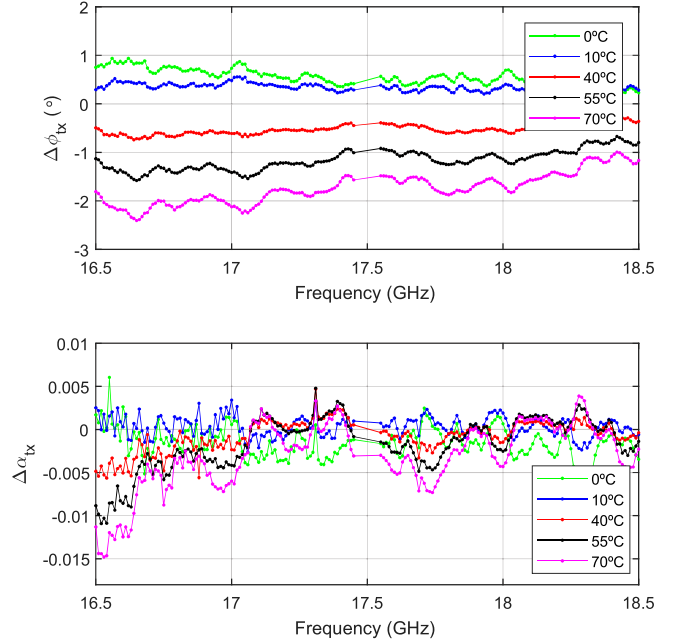


Fig. 8. Temperature impact on gain and phase imbalance.

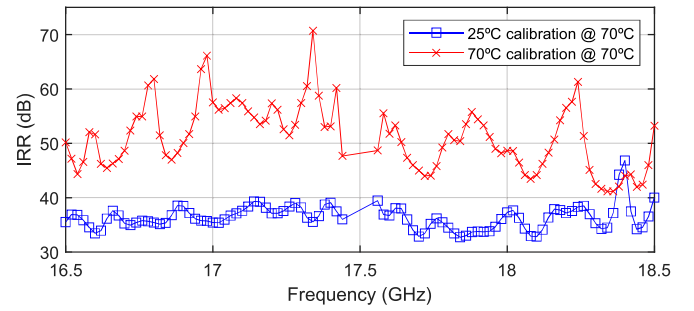


Fig. 9. Postcalibration IRR performance.

performed at 70 °C. We can observe a decrease in the IRR in whole band of the signal. In average, there is a reduction of around 15 dB. Thus, we can conclude that the postcalibration performance is significantly deteriorated, as temperature varies. Temperature drifts have the potential to degrade the performance in a meaningful way, and thus, these drifts need to be carefully tracked and considered for I/Q imbalance compensation, especially for high modulation orders (>64 QAM) and wideband channels (>1 GHz).

As it was explained in Section II, two individual sub-QAM signals are modulated and transmitted, each one with a bandwidth of 1 GHz. DS0 is centered at -500 MHz and DS1 at 500 MHz, which, in IF, correspond to 17 and 18 GHz, respectively. DS0 spans from 16.5 to 17.5 GHz and its mirror frequencies from 17.5 to 18.5 GHz, i.e., in the bandwidth occupied by DS1. Likewise, the mirror frequencies of DS1 fall exactly in the frequency band where DS0 is transmitted. Thus, when the whole signal is transmitted, the image components can not be seen by just looking at the output spectrum.

In order to show the impact of the temperature during the transmission of the whole signal, the digital baseband processor can be set to transmit only DS0 or DS1, which allows its image component to be seen. When only DS0 is

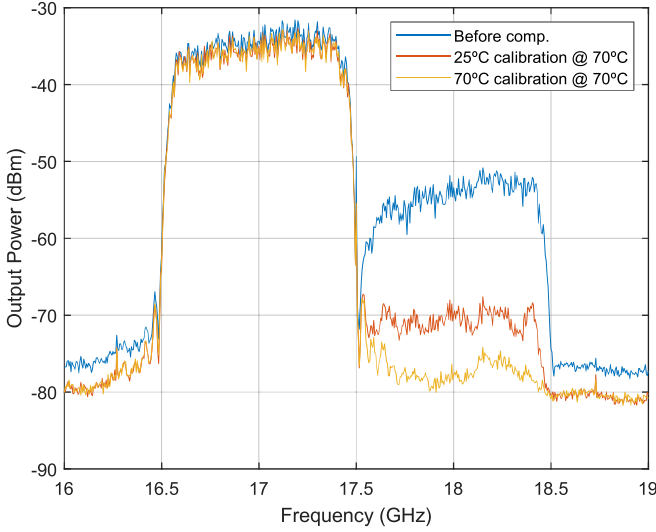


Fig. 10. Spectrum of DS0 in IF.

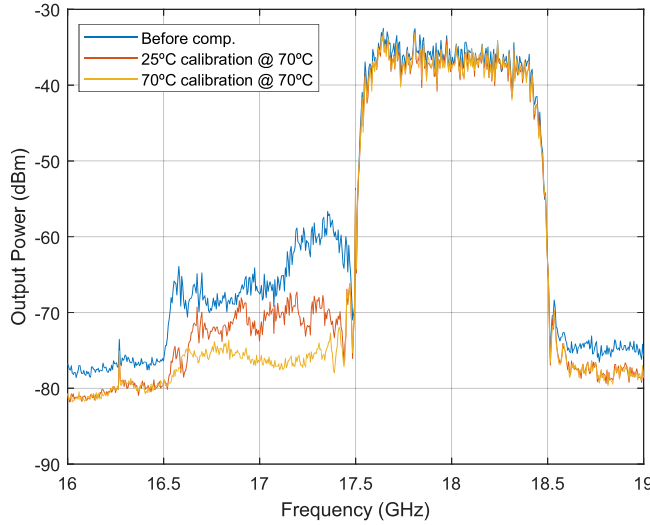


Fig. 11. Spectrum of DS1 in IF.

transmitted, the waveform shown in Fig. 10 is obtained. The spectrum labeled “Before comp.” corresponds to the case without compensation. In this case, the image signal caused by I/Q imbalance can be easily appreciated between 17.5 and 18.5 GHz, exactly where the DS1 would be transmitted. In the case where the transmitter is operating at the temperature at which it was calibrated (spectrum labeled “70 °C estimation at 70 °C”), the figure shows that the image signal is rejected, since it is almost at the level of the noise floor. It can be seen that IRR values of more than 35 dB are obtained. Note that an IRR requirement of 35 dB was reported in [29] for this system. However, when operating at a different temperature from the one at calibration (spectrum labeled “25 °C estimation at 70 °C”), the image between 17.5 and 18.5 GHz can be clearly appreciated. This image would be seen as noise corrupting DS1 and it would degrade the performance of our system. A similar conclusion can be reached by observing Fig. 11, which represents the case when DS1 is being transmitted. Based on these measurements, we can conclude

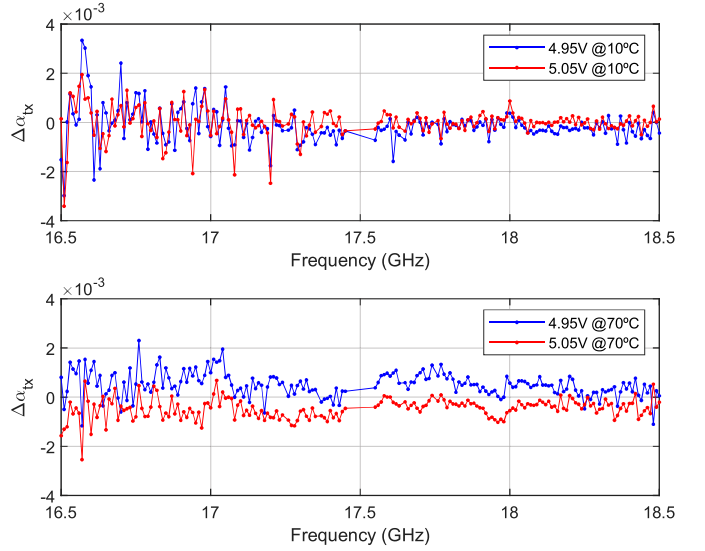


Fig. 12. Supply voltage impact on gain imbalance at 10 °C and 70 °C.

that temperature variations result in a significant reduction in the performance of our system.

In order to ensure that the test setup is robust and all the observed changes in the I/Q imbalance are mostly due to temperature variations, the sensitivity to small voltage variations is analyzed due to significant temperature variations, process drift, or aging of circuit components, especially low-dropout (LDO) regulators.

In order to do so, the measurement setup shown in Fig. 3 and explained in Section III was used. In the analog front end shown in Fig. 5(a), the GaAs I/Q upconverter is the only active component, which is fed with a supply voltage of 5 V. Thus, in order to evaluate the impact of voltage variations, the feeding supply voltage of the I/Q modulator is varied. Variations of  $\pm 1\%$  of the feeding voltage are considered, which is the typical range achievable by low-cost commercial LDOs [33]. In order to analyze the combined effect of the feeding voltage and temperature over I/Q imbalance, the analog front end was introduced in the temperature chamber, as shown in Fig. 3, and measurements were performed at 10 °C and 70 °C.

Figs. 12 and 13 show the impact that the feeding voltage has on gain and phase imbalance curves, respectively, when the transmitter is at 10 °C and 70 °C. The figures show the gain and phase imbalance curves relative to the curves at 5 V. Fig. 12 shows that in the considered I/Q upconverter, the gain imbalance is not sensitive to feeding voltage variations for the test temperatures (10 °C–70 °C). The same conclusions can be applied to the phase imbalance, as negligible variations are observed in the curves shown in Fig. 13. Thus, it is concluded that the observed changes in the I/Q imbalance are mainly caused by temperature variations.

#### B. Measurement Results With 55-nm BiCMOS Upconverter

The analog front end shown in Fig. 5(a) is now replaced by the one in Fig. 5(b) in order to analyze whether the observed behavior of I/Q imbalance over temperature is repeatable in other systems.

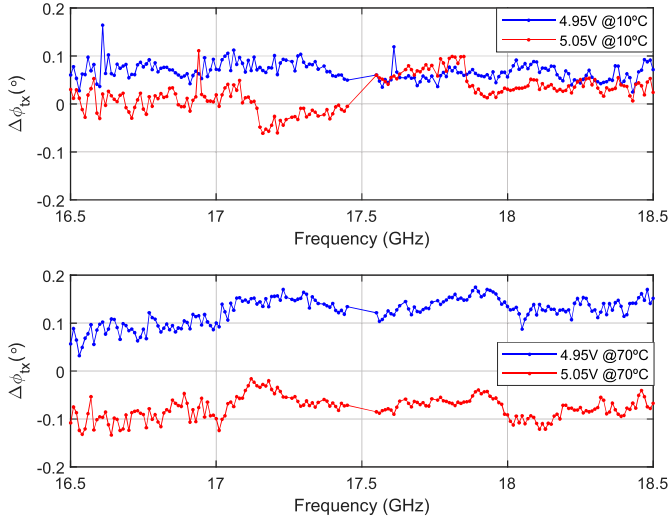


Fig. 13. Supply voltage impact on phase imbalance at 10 °C and 70 °C.

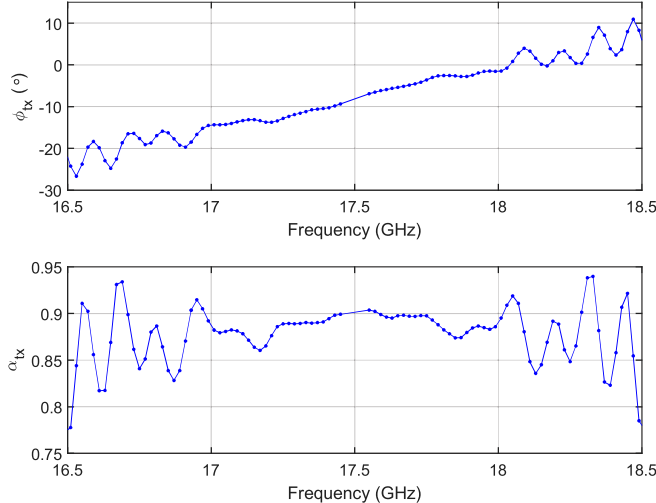


Fig. 14. I/Q gain and phase imbalance for a 55-nm BiCMOS upconverter

Fig. 14 represents the measured I/Q phase ( $\phi_{tx}$ ) and gain ( $\alpha_{tx}$ ) imbalance over the whole band of frequency. Again, we can appreciate a frequency-dependent behavior of I/Q imbalance. Fig. 15 shows the measured IRR of the analog front end before and after compensation. It can be observed that the IRR is enhanced in the whole band, achieving values above 40 dB, as it was in the case with the GaAs upconverter.

Fig. 16 shows the gain and phase imbalance curves for different temperatures compared to the gain and phase imbalance curves at 25 °C. The phase imbalance curves show smaller variations over temperature compared to the GaAs upconverter. Nonetheless, higher gain imbalance variations are observed. In any case, both gain and phase imbalance curves show a shifting behavior with temperature, as it was observed in Section IV-A.

Based on the measurements performed in this section, we can draw the following conclusions. First, feeding voltage variations of  $<\pm 1\%$  are shown to have insignificant effects on gain and phase imbalance at any temperature. Second, temperature variations have a significant impact on

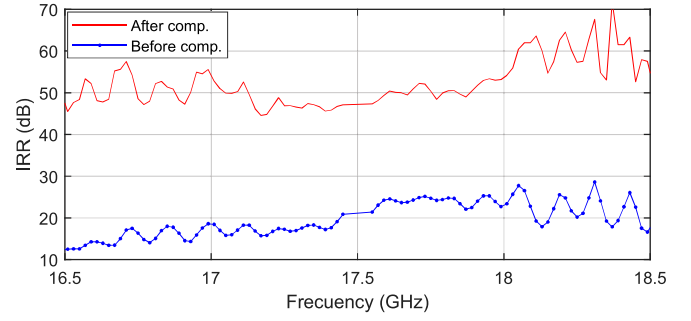


Fig. 15. IRR before and after compensation for a 55-nm BiCMOS upconverter.

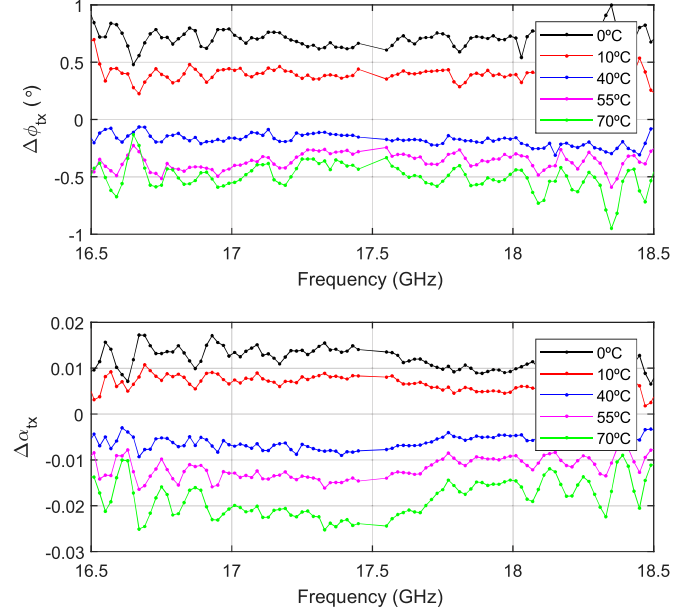


Fig. 16. Temperature impact on gain and phase imbalance using a 55-nm BiCMOS upconverter.

the I/Q imbalance characteristics. Thus, Section V proposes an approach that considers these temperature drifts in the I/Q imbalance compensation. Such an approach should ideally be able to compensate for I/Q imbalance without interrupting the data transmission.

## V. TEMPERATURE-DEPENDENT I/Q IMBALANCE COMPENSATION

### A. Proposed Approach

It was observed that drifts in ambient temperature trigger changes in the transmitter behavior. Fig. 17 shows the gain and phase imbalance over the temperature for different frequencies of the signal band when the GaAs upconverter was used, whereas Fig. 18 shows the corresponding SiGe BiCMOS upconverter. As a first approximation, it can be assumed a linear behavior with temperature for each frequency. Given this observation, we just need to have two gain and phase imbalance characteristics of the entire frequency band for the estimation at any temperature.

Thus, let us suppose that a factory calibration of the transmitter is done at two different temperatures, i.e.,  $T_1$  and  $T_2$ .

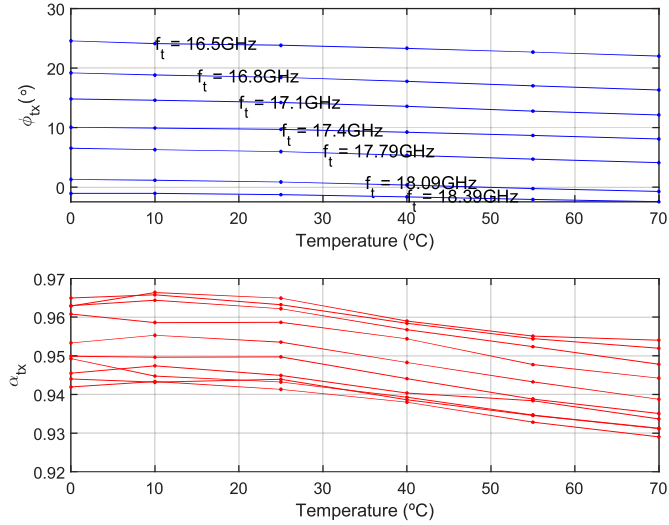


Fig. 17. Gain and phase imbalance as a function of the temperature using GaAs upconverter.

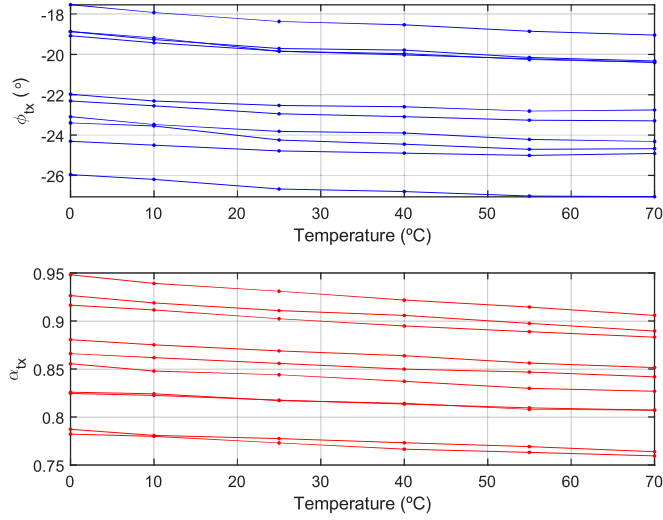


Fig. 18. Gain and phase imbalance as a function of the temperature using SiGe BiCMOS upconverter.

From these calibrations, we obtain two curves of gain imbalances,  $\alpha_{T_1}(f)$  and  $\alpha_{T_2}(f)$ , and two curves of phase imbalances,  $\phi_{T_1}(f)$  and  $\phi_{T_2}(f)$ . By linearly interpolating these set of curves, an estimation of the phase and gain imbalance can be obtained at any temperature. An estimation of the phase mismatch is obtained with (3), while (4) estimates the gain mismatch

$$\hat{\phi}_T(f_t) = \frac{\phi_{T_1}(f_t)[T_2 - T] + \phi_{T_2}(f_t)[T - T_1]}{T_2 - T_1} \quad (3)$$

$$\hat{\alpha}_T(f_t) = \frac{\alpha_{T_1}(f_t)[T_2 - T] + \alpha_{T_2}(f_t)[T - T_1]}{T_2 - T_1}. \quad (4)$$

Therefore, once the system is powered up, we just need to measure the temperature at which the system is working,  $T$ . If DSP-TX stores a lookup table with the coefficients of the precompensator filter at different temperatures, we can select the coefficients in the LUT corresponding to the closest temperature to the measured temperature.

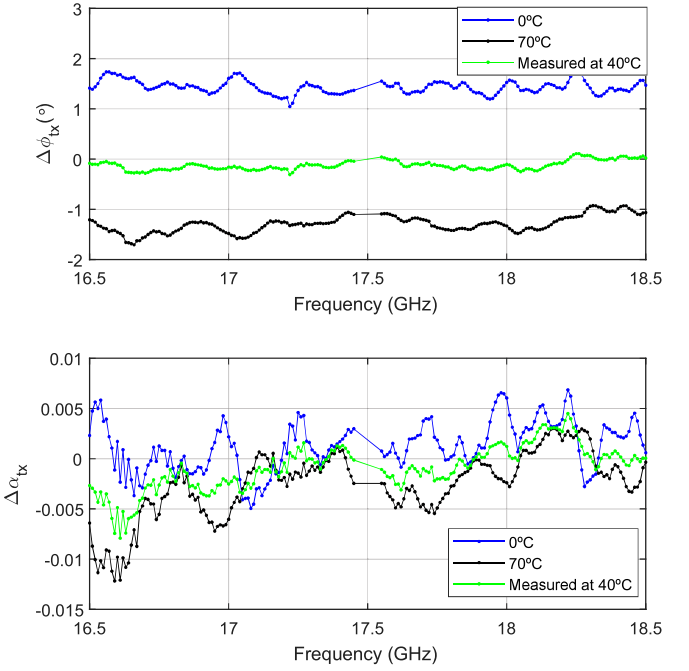


Fig. 19. Gain and phase imbalance estimation error.

### B. Performance Evaluation

This section evaluates the effectiveness of the proposed calibration technique. To do so, the test setup described in Section III with the GaAs upconverter was used.

Fig. 19 shows different gain and phase imbalance curves over the frequency band relative to the gain and phase imbalance curves measured at 40 °C. For example, the curves labeled “70 °C” are defined as follows:

$$\Delta\phi_{tx70^\circ} = \phi_{tx70^\circ}(f) - \phi_{tx40^\circ}(f) \quad (5)$$

$$\Delta\alpha_{tx70^\circ} = \alpha_{tx70^\circ}(f) - \alpha_{tx40^\circ}(f). \quad (6)$$

The curves measured at 0 °C and 70 °C were used as a reference to estimate the mismatches at 40 °C. The curves labeled “Measured at 40 °C,” which should ideally be zero, show the gain and phase imbalance at 40 °C estimated using (3) and (4), where  $T_1 = 0$  °C and  $T_2 = 70$  °C,  $\phi_{T_1}(f)$ , and  $\phi_{T_2}(f)$  are the phase imbalance curves at 0 °C and 70 °C, and  $\alpha_{T_1}(f)$  and  $\alpha_{T_2}(f)$  are the gain imbalance curves at 0 °C and 70 °C. It can be observed that the estimated imbalances at 40 °C are very similar to the imbalances measured at this temperature, since the curve labeled “Measured at 40 °C” is almost zero for the whole band. Thus, it can be concluded that both gain and phase imbalances can accurately be calculated with the proposed method.

The curve labeled “Estimated” in Fig. 20 represents the measured IRR when the gain and phase imbalance were estimated with the proposed method, i.e., using (3) and (4). On the other hand, the curve labeled “Recalibrated” was measured after performing a new calibration at 40 °C. Fig. 20 shows that when using the measured and the estimated curves, analogous IRRs are reached: in average, 51 dB for the “Recalibrated” case and 50 dB for the “Estimated” one. Therefore, we can

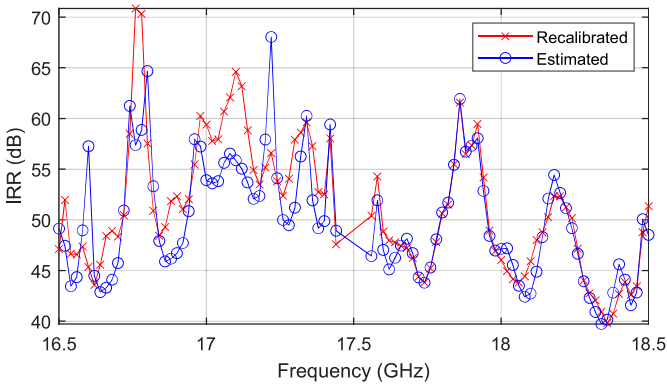


Fig. 20. Estimated versus measured IRR.

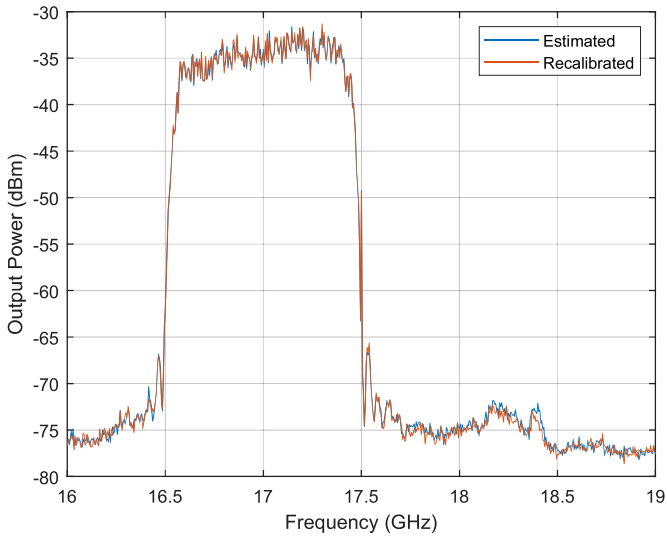


Fig. 21. DS0 spectrum before and after compensation.

conclude that the undesired image components can be precisely rejected when using the estimated gain and phase imbalances. Looking at Fig. 9, we can see an improvement of 15 dB compared to not performing any temperature calibration.

Finally, Fig. 21 represents the spectrum when DS0 is transmitted. If we compensate the I/Q imbalance with the proposed technique, the spectrum labeled “Estimated” is obtained. In this case, it is shown that the undesired image is reduced almost to the level of the noise floor. For comparison purposes, this figure also shows the spectrum obtained when the I/Q imbalance is compensated applying a new calibration, the spectrum labeled “Recalibrated.” Comparing both spectrums, negligible differences are appreciated, which confirms that the proposed approach is accurate enough. This claim can also be confirmed by observing Fig. 22, which shows the spectrum when DS1 is transmitted. Fig. 23 shows the relative difference between both spectrums, considering together the image signals of DS0 and DS1. The mean error is lower than 1 dB, which confirms that the proposed estimation technique can be considered as accurate as recalibrating the system.

These results confirm that the proposed approach is able to accurately compensate the temperature-dependent I/Q imbalance using only a two temperature point factory calibrations of gain and phase imbalance.

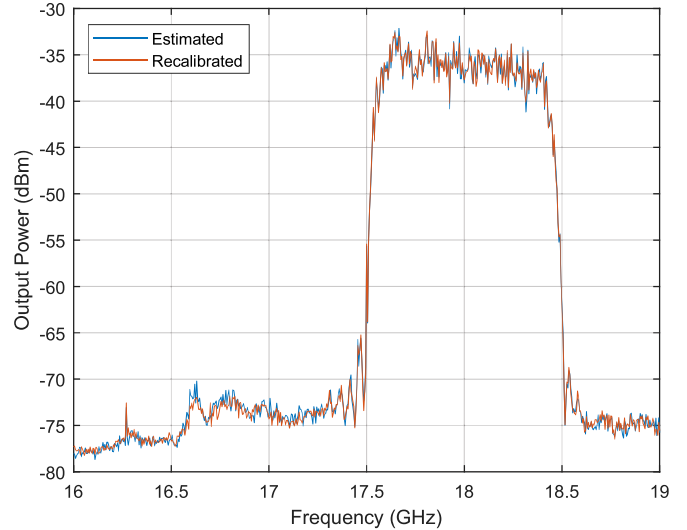


Fig. 22. DS1 spectrum before and after compensation.

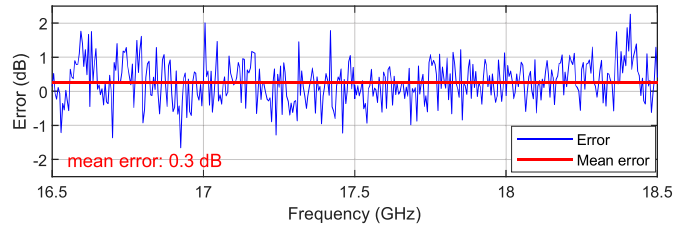


Fig. 23. Error between the estimated and the recalibrated spectrums.

### C. Cost of the Proposed Method

As it was already mentioned, DSP-TX stores the coefficients of the precompensator filter at different temperatures in lookup tables. The size of these tables will depend on the number of temperatures considered and the number of coefficients of the precompensator.

Regarding the required number of temperatures, let us suppose that we set a step of 10 °C between each set of temperature. From the data in Fig. 17, a change of 10 °C results in a phase imbalance of slightly less than 0.3° and a gain imbalance of around 0.005. These values of gain and phase imbalance result in an IRR of around 50 dB, which is well above the IRR required for the considered application. Thus, with a step of 10 °C between temperatures, the possible degradation due to a discrete vector of temperatures will be negligible. In order to cover the temperature range from 0 °C to 70 °C with a step of 10 °C, the LUT would contain eight sets of coefficients.

Regarding the number of coefficients, the size of the LUT grows linearly with the order of the filter. For a filter of order  $N$ , the LUT will have  $(N + 1)W$  bits for each temperature, where  $W$  is the word size of the coefficient. For the measurements presented in this article, the precompensator filter was working with 21 taps. Reducing the number of taps will directly reduce the size of the LUTs and the FPGA consumption, but it will compromise the performance of the I/Q imbalance compensation.

Regarding calibration time, compared to I/Q imbalance calibration techniques that only account for process variations,

such as the ones in [6] and [29], the proposed method doubles the calibration time.

#### D. Enhancement of the Proposed Approach

In Section V-A, it was concluded that, in the considered system, phase and gain imbalances over frequency and temperature can be well approximated using a linear model. In fact, from Fig. 17, it can be deduced that drifts in temperature do not change the shape of the imbalance curves, as the slopes are very similar. This observation agrees with the shifting behavior observed in Section IV. Because of this, it could be possible to map the I/Q imbalance at any operating temperature without the need to have two complete sets of gain and imbalance curves, but only one set of curves and the rate at which the imbalances decrease with temperature.

Modeling the relationship between the imbalances and temperature as linear and with the same slope for all frequencies, the phase and gain imbalance can be written as a function of the temperature with (7) and (8).  $K_\phi$  is the proportionality factor between temperature and phase imbalance,  $K_\alpha$  is the proportionality factor between temperature and gain imbalance, and  $\phi_{T_1}(f)$  and  $\alpha_{T_1}(f)$  are, respectively, the phase and gain imbalance curves obtained when calibrating the system at a temperature  $T_1$

$$\hat{\phi}_T(f_t) = \phi_{T_1}(f_t) + K_\phi(T - T_1) \quad (7)$$

$$\hat{\alpha}_T(f_t) = \alpha_{T_1}(f_t) + K_\alpha(T - T_1). \quad (8)$$

To calculate the values of the proportionality factors,  $K_\phi$  and  $K_\alpha$ , only the phase and gain imbalance at one frequency,  $f_t$ , at two different temperatures are required.

Let us suppose that a factory calibration is done at a temperature  $T_1$ . From this calibration,  $\phi_{T_1}(f)$  and  $\alpha_{T_1}(f)$  are obtained. In addition, let us assume that we measure the phase and gain imbalance at a frequency,  $f_t$ , at a second temperature,  $T_2$ . The slope between these two points corresponds to the proportionality factor. Thus,  $K_\phi$  and  $K_\alpha$  can be computed with the following equations:

$$K_\phi = \frac{\phi_{T_2}(f_t) - \phi_{T_1}(f_t)}{T_2 - T_1} \quad (9)$$

$$K_\alpha = \frac{\alpha_{T_2}(f_t) - \alpha_{T_1}(f_t)}{T_2 - T_1}. \quad (10)$$

With only these measurements, we can estimate the gain and phase imbalance curves at the operating temperature,  $T$ , following (7) and (8). This method, compared to the first approach, reduces in  $\sim 50\%$  the number of measurements that need to be done in order to characterize the I/Q imbalance. Thus, the increment in calibration time is  $< 2\%$  compared to I/Q imbalance calibration techniques that only account for process variations [6].

#### E. Comparison of Proposed Methods

In this section, the proposed methods are compared by analyzing the accuracy of the performance obtained with each method. To do so, the measurement setup described in Section III was used.

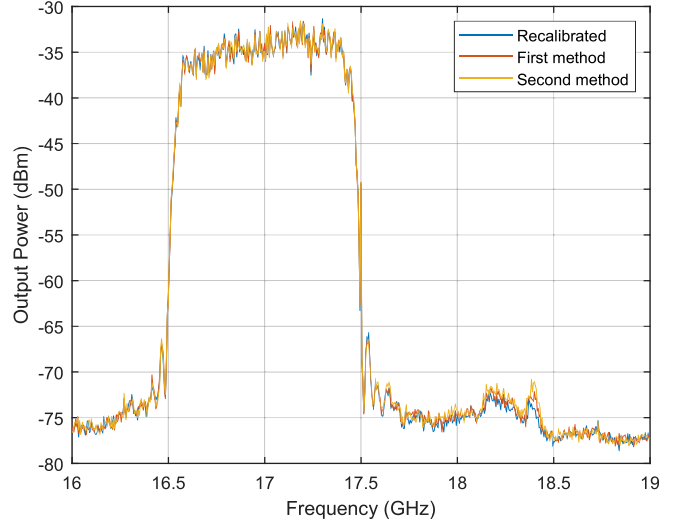


Fig. 24. DS0 spectrum after compensation with different methods at 40 °C.

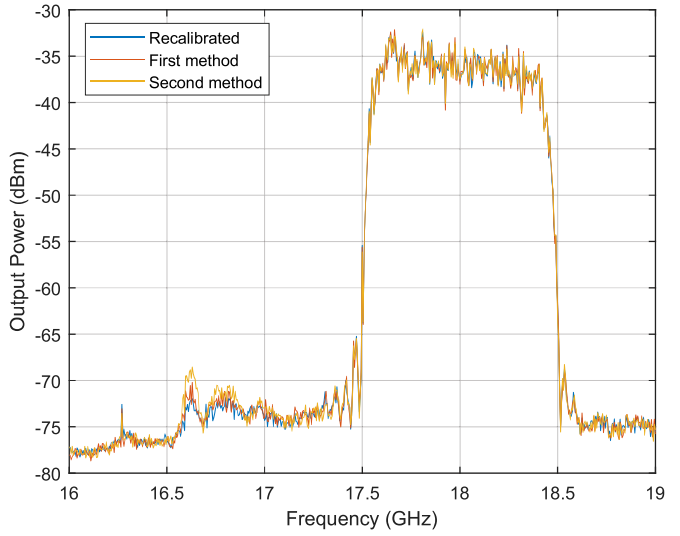


Fig. 25. DS1 spectrum after compensation with different methods at 40 °C.

Figs. 24 and 25 show the spectrum when DS0 and DS1 are separately transmitted, respectively. The figures show the obtained spectrum with the proposed methods. It is shown that in both the cases, the image produced by the I/Q imbalance is well attenuated, as the image is rejected in more than 35 dB in the whole signal bandwidth. For comparison purposes, the recalibrated spectrum is also depicted. It should be noted that the spectrum obtained when recalibrating the system and the ones obtained with the proposed methods are almost identical.

Finally, the MER and EVM of the transmitted signal are measured, so as to compare the performance and accuracy obtained with each method. In order to do so, 100 000 symbols are transmitted concurrently through DS0 and DS1. The obtained IF signal is downconverted to a low-IF of 1.25 GHz using a commercial I/Q downconverted (Hittite HMC966LP4E) and this signal is captured using a high-speed digital oscilloscope (DSO9104A), as it is shown in [6]. The signal captured by the oscilloscope is demodulated in

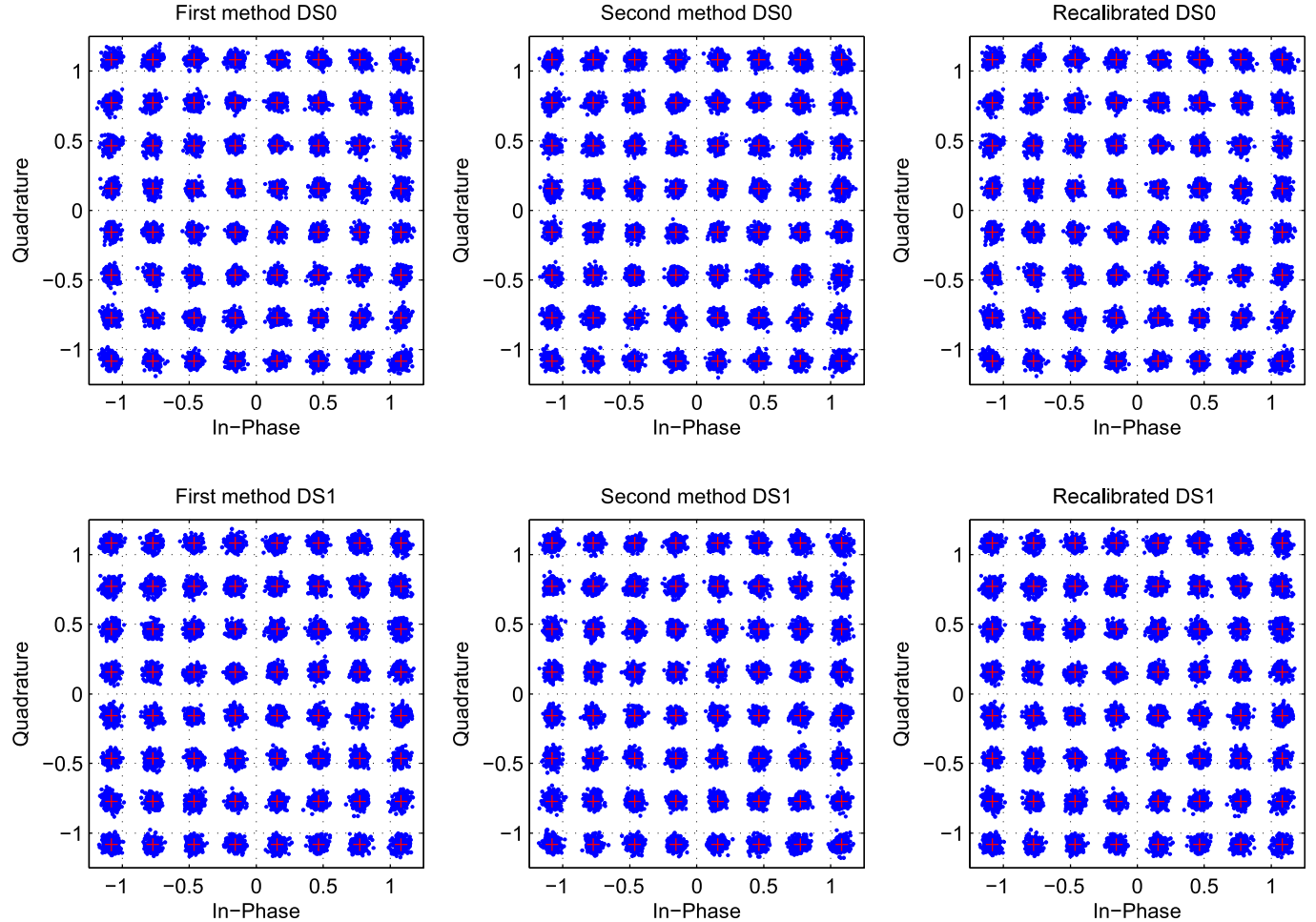


Fig. 26. Constellations after compensation with different methods.

TABLE I  
EVM AND MER RESULTS<sup>1</sup>

	EVM (%)		MER (dB)	
	DS0	DS1	DS0	DS1
<b>Before comp.</b>	3.4	7.0	25.7	19.5
<b>First method</b>	2.5	2.7	28.4	27.8
<b>Second method</b>	2.6	2.7	28.1	27.8
<b>Recalibrated</b>	2.5	2.8	28.5	27.2

<sup>1</sup>Normalized to the peak constellation power.

MATLAB, but this time, DS0 and DS1 are separately demodulated. Fig. 26 shows the obtained constellation diagrams, where the red crosses are the reference 64-QAM symbols, while the blue dots are the received symbols. The constellations in the top row correspond to the DS0 signal and the ones in the bottom row to the DS1 signal. The first two columns correspond to the proposed methods and the last one to the recalibrated case. In order to quantify the differences between the three constellations, the EVM and the MER of each constellation are illustrated in Table I. It is shown that the distortion produced by I/Q imbalance is reduced by recalibrating the system or using any of the proposed methods.

As a matter of fact, an improvement of more than 8 dB is observed in the MER of DS1.

It is worth noting that we can obtain a very similar performance with any of the proposed compensation techniques and recalibrating the system. With the proposed methods, the EVM is around 2.6% and the MER around 28 dB. This proves that the proposed techniques are accurate enough to compensate for I/Q imbalance at any temperature without the need to recalibrate the system.

## VI. CONCLUSION

This article analyzes the influence of temperature variations over the I/Q imbalance of a wideband transmitter. It was shown that temperature drifts cause significant gain and phase imbalance variations. Consequently, if the I/Q imbalance was estimated at a different temperature than the one at which the system is operational, the IRR can be reduced in more than 15 dB and, thus, the overall system performance can be deteriorated.

In order to cope with this issue, this article presents a temperature-dependent I/Q imbalance precompensation method able to compensate for frequency-dependent I/Q imbalance in wideband transmitters over the whole temperature range. The method only needs a couple of gain and

phase imbalance characteristics that could be performed as factory calibrations in order to estimate the I/Q imbalance at any temperature. In order to maintain the IRR at appropriate levels, the temperature must be monitored and corresponding changes must be made in the I/Q imbalance compensation routine. In addition, the proposed estimation method can be enhanced by taking advantage of the linear behavior and equal slopes observed in temperature-dependent imbalance curves in the whole signal bandwidth. This enables performing the estimation with less information, which ultimately means a faster calibration.

The proposed technique is validated through measurements in a wideband TRx using 64-QAM modulation and a bandwidth of 2 GHz. The results show that the proposed methods are able to obtain a precise characterization of the gain and phase imbalance and thus, are able to accurately compensate an impaired transmitter. The obtained results lead to the conclusion that the proposed temperature-dependent I/Q imbalance compensation methods are as effective as recalibrating the system when temperature drifts are detected with the advantage that the proposed methods avoid interrupting the normal operation of the system. The measurements show that the proposed approach is able to keep the IRR greater than 35 dB in the entire bandwidth and an EVM lower than 3% over a temperature range of 70 °C.

## REFERENCES

- [1] V. Wong, R. Schober, D. Ng, and L. Wang, *Key Technologies for 5G Wireless Systems*. Cambridge, U.K.: Cambridge Univ. Press, 2017.
- [2] M. Valkama, A. Springer, and G. Hueber, “Digital signal processing for reducing the effects of RF imperfections in radio devices—An overview,” in *Proc. IEEE Int. Symp. Circuits Syst.*, May 2010, pp. 813–816.
- [3] E. Cetin, I. Kale, and R. C. S. Morling, “Living and dealing with RF impairments in communication transceivers,” in *Proc. IEEE Int. Symp. Circuits Syst.*, May 2007, pp. 21–24.
- [4] G. Fettweis, M. Lohning, D. Petrovic, M. Windisch, P. Zillmann, and W. Rave, “Dirty RF: A new paradigm,” in *Proc. IEEE 16th Int. Symp. Pers., Indoor Mobile Radio Commun. (PIMRC)*, vol. 4, Sep. 2005, pp. 2347–2355.
- [5] A. Rezola, J. Sevillano, D. del Río, I. Gurutzeaga, R. Berenguer, and I. Velez, “Frequency-selective IQ imbalance in zero-second-IF transceivers for wide-band mmW links,” in *Proc. 19th Int. Conf. Circuits, Syst., Commun. Comput. (CSCC)*, 2015, pp. 98–104.
- [6] A. Rezola *et al.*, “Built-in-self-calibration for I/Q imbalance in wideband millimeter-wave gigabit transmitters,” *IEEE Trans. Microw. Theory Techn.*, vol. 65, no. 11, pp. 4758–4769, Nov. 2017.
- [7] F. Piri, M. Bassi, N. R. Lacaita, A. Mazzanti, and F. Svelto, “A PVT-tolerant >40-dB IRR, 44% fractional-bandwidth ultra-wideband mm-wave quadrature LO generator for 5G networks in 55-nm CMOS,” *IEEE J. Solid-State Circuits*, vol. 53, no. 12, pp. 3576–3586, Dec. 2018.
- [8] J. Y.-C. Liu *et al.*, “Smart RF integrated circuits: A millimeter-wave gigabit transceiver with digitally-enabled built-in self-healing and auto-switching functions,” *IEEE Microw. Mag.*, vol. 20, no. 1, pp. 28–37, Jan. 2019.
- [9] J. Pang *et al.*, “A 50.1-Gb/s 60-GHz CMOS transceiver for IEEE 802.11ay with calibration of LO feedthrough and I/Q imbalance,” *IEEE J. Solid-State Circuits*, vol. 54, no. 5, pp. 1375–1390, Jan. 2019.
- [10] D. Zhao and P. Reynaert, “A 40 nm CMOS E-band transmitter with compact and symmetrical layout floor-plans,” *IEEE J. Solid-State Circuits*, vol. 50, no. 11, pp. 2560–2571, Nov. 2015.
- [11] P. Ramabadran *et al.*, “Digitally assisted wideband compensation of parallel RF signal paths in a transmitter,” in *Proc. ARFTG Microw. Meas. Conf.*, Jun. 2018, pp. 1–4.
- [12] A. Chung, M. B. Rejeb, Y. Beltagy, A. M. Darwish, H. A. Hung, and S. Boumaiza, “IQ imbalance compensation and digital predistortion for millimeter-wave transmitters using reduced sampling rate observations,” *IEEE Trans. Microw. Theory Techn.*, vol. 66, no. 7, pp. 3433–3442, Jul. 2018.
- [13] R. Moorti and J. Hammerschmidt, “Receiver IQ imbalance calibration,” U.S. Patent 2007 0025474 A1, Jul. 29, 2005. [Online]. Available: <https://patents.google.com/patent/US20070025474>
- [14] O. Mylläri, L. Anttila, and M. Valkama, “Digital transmitter I/Q imbalance calibration: Real-time prototype implementation and performance measurement,” in *Proc. 18th Eur. Signal Process. Conf.*, Aug. 2010, pp. 537–541.
- [15] M. Pospišil, R. Maršálek, and T. Gothans, “Wireless device classification through transmitter imperfections—Evaluation of performance degradation due to the chip heating,” in *Proc. IEEE Radio Wireless Symp. (RWS)*, Jan. 2017, pp. 169–172.
- [16] S. Y. Chen and J.-S. Yuan, “Adaptive gate bias for power amplifier temperature compensation,” *IEEE Trans. Device Mater. Rel.*, vol. 11, no. 3, pp. 442–449, Sep. 2011.
- [17] Y. Zhang and J.-S. Yuan, “CMOS transistor amplifier temperature compensation: Modeling and analysis,” *IEEE Trans. Device Mater. Rel.*, vol. 12, no. 2, pp. 376–381, Jun. 2012.
- [18] N. Wolf, J.-E. Mueller, and H. Klar, “Simple predistortion system for compensation of temperature dependent nonlinearity of power amplifiers,” in *Proc. IEEE Radio Wireless Symp. (RWS)*, Jan. 2010, pp. 152–155.
- [19] (2014). *Phase Shifters and I-Q Modulators*. [Online]. Available: <http://www.admiral-microwaves.co.uk/pdf/herley/herley-catalogue-phase-shifters.pdf>
- [20] D. del Río *et al.*, “A wideband and high-linearity E-B and transmitter integrated in a 55-nm SiGe technology for backhaul point-to-point 10-Gb/s links,” *IEEE Trans. Microw. Theory Techn.*, vol. 65, no. 8, pp. 2990–3001, Aug. 2017.
- [21] S. Mirabbasi and K. Martin, “Hierarchical QAM: A spectrally efficient DC-free modulation scheme,” *IEEE Commun. Mag.*, vol. 38, no. 11, pp. 140–146, Nov. 2000.
- [22] A. Rezola *et al.*, “Non-frequency-selective I/Q imbalance in zero-IF transceivers for wide-band mmW links,” in *Proc. 10th Int. Conf. Wireless Mobile Commun. (ICWMC)*, 2014, pp. 136–141.
- [23] A. Rezola, “Design and implementation of I/Q imbalance compensation methods in UWB multi-Gbps transmitters for point-to-point communications,” Ph.D. dissertation, ICT Division, Univ. Navarra, Pamplona, Spain, 2017.
- [24] L. Anttila, M. Valkama, and M. Renfors, “Frequency-selective I/Q mismatch calibration of wideband direct-conversion transmitters,” *IEEE Trans. Circuits Syst. II, Exp. Briefs*, vol. 55, no. 4, pp. 359–363, Apr. 2008.
- [25] J. Luo, A. Kortke, W. Keusgen, and M. Valkama, “A novel adaptive calibration scheme for frequency-selective I/Q imbalance in broadband direct-conversion transmitters,” *IEEE Trans. Circuits Syst. II, Exp. Briefs*, vol. 60, no. 2, pp. 61–65, Feb. 2013.
- [26] K. S. Lorenz, J. Goodman, G. Stantchev, and N. A. Pendergrass, “Generalized transmitter compensation of frequency dependent I/Q imbalance,” *IEEE Trans. Signal Process.*, vol. 64, no. 9, pp. 2220–2231, May 2016.
- [27] E. Tsui and J. Lin, “Adaptive IQ imbalance correction for OFDM systems with frequency and timing offsets,” in *Proc. IEEE Global Telecommun. Conf. (GLOBECOM)*, vol. 6, Nov. 2004, pp. 4004–4010.
- [28] H. Zareian and V. T. Vakili, “New adaptive method for IQ imbalance compensation of quadrature modulators in predistortion systems,” *EURASIP J. Adv. Signal Process.*, vol. 2009, p. 37, Jan. 2009.
- [29] D. del Río, A. Rezola, J. Sevillano, I. Velez, and R. Berenguer, *Digitally Assisted, Fully Integrated, Wideband Transmitters for High-Speed Millimeter-Wave Wireless Communication Links*. New York, NY, USA: Springer, 2018.
- [30] E. Nash, “Correcting imperfections in IQ modulators to improve RF signal fidelity,” Analog Devices, Norwood, MA, USA, Appl. Note 1039, 2009.
- [31] 7 Series FPGAs Data Sheet: Overview (DS180), Rev. 2.6, Xilinx, San Jose, CA, USA, Feb. 2018.
- [32] 11-/14-Bit, 5.7 GSPS, RF Digital-to-Analog Converter, Rev. B, Analog Devices, Norwood, MA, USA, Feb. 2017.
- [33] ON Semiconductor. (2014). 1.0 A Low-Dropout Positive Fixed and Adjustable Voltage Regulators, Rev. 4. [Online]. Available: <https://www.onsemi.com/pub/Collateral/NCP1117LP-D.pdf>



**Ainhoa Rezola** was born in Donostia-San Sebastian, Spain, in 1990. She received the M.Sc. degree in telecommunication engineering and the Ph.D. degree in applied engineering from TECNUN—University of Navarra, Donostia-San Sebastian, in 2013 and 2017, respectively.

Since 2013, her research has focused on the design of digital systems, especially on the design and implementation of hardware platforms based on microprocessors and FPGAs. She joined the Electronic and Communication Department, Ceit-IK4 Research Centre, Donostia-San Sebastian, in 2013. She is currently a Lecturer with TECNUN—University of Navarra. Since 2013, she has authored or coauthored numerous articles in national and international conferences, as well as in specialized journals. She has also authored a technical book and holds an international patent.



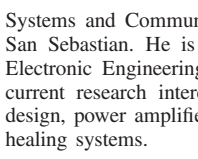
**Juan F. Sevillano** (M'08–SM'18) received the M.Sc. degree in electrical, electronic, and control engineering and the Ph.D. degree from the University of Navarra, Pamplona, Spain, in 1999 and 2004, respectively.

In 2000, he joined the Ceit-IK4 Research Centre, Donostia-San Sebastian, Spain, where he is involved in projects related to wireless communications and sensor systems. He is also a Lecturer with TECNUN—University of Navarra, Donostia-San Sebastian. His research interests include signal processing and the implementation of electronic systems.



**David del Río** (GS'14–M'18) was born in Donostia-San Sebastian, Spain, in 1990. He received the M.Sc. and Ph.D. degrees in telecommunication engineering from TECNUN—University of Navarra, Donostia-San Sebastian, in 2013 and 2017, respectively.

In 2016, he was a Visiting Graduate Researcher with the High Speed Electronics Laboratory, University of California at Los Angeles, Los Angeles, CA, USA, where he was involved in the design of integrated transceivers for 5G communications. He is currently a Researcher with the Electronics Systems and Communications Group, Ceit-IK4 Research Centre, Donostia-San Sebastian. He is also an Associate Professor with the Electrical and Electronic Engineering Department, TECNUN—University of Navarra. His current research interests include millimeter-wave (mmW) and RF circuit design, power amplifiers, phased arrays, and reconfigurable devices for self-healing systems.



**Belén Martín** was born in Donostia-San Sebastian, Spain, in 1996. She received the B.S. degree in telecommunications systems engineering from TECNUN—University of Navarra, Donostia-San Sebastian, in 2018, where she is currently pursuing the M.Sc. degree in telecommunication engineering.

She has been a Research Assistant with the Digital Signal Processing Group, Ceit-IK4 Research Centre, Donostia-San Sebastian, and the Design and Analysis of Deep Neural Networks Group, Fraunhofer IIS, Erlangen, Germany, in 2018. Her research interests include wireless systems.



**Iñaki Gurutzeaga** was born in Hernani, Spain. He received the M.Sc. degree in telecommunication engineering from the Polytechnic University of Catalonia, Barcelona, Spain, in 1992, and the Ph.D. degree in ultra-wideband devices for broadband communication systems at microwave frequencies from TECNUN—University of Navarra, Donostia-San Sebastian, Spain, in December 2008.

He has 18 years of experience as a Researcher and Product Manager in RF and microwave fields with three different companies: Fagor Electronica S. Coop., ALCAD S.A., and IKUSI S.A. Since 2003, he has been a Lecturer with TECNUN—University of Navarra, where he is involved in devices and circuits of microwaves, and a Research Scientist of integrated circuit (IC) design and antennas with the Sensor and Analogue Electronics Group (SAE), ICT Division, Ceit-IK4 Research Centre, Donostia-San Sebastian. He is involved in diverse projects in  $\mu\text{W}$  and mmW frequencies, up to subterahertz frequencies.



**Igone Vélez** (M'06) received the M.Sc. degree in electrical, electronic, and control engineering and the Ph.D. degree from the University of Navarra, Pamplona, Spain, in 2000 and 2005, respectively.

She has been a Research Staff Member with the Ceit-IK4 Research Centre, Donostia-San Sebastian, since 2000, and an Associate Professor with the University of Navarra since 2005. She is currently the Director of the ICT Division, Ceit-IK4 Research Centre. She has been involved in international and national projects related to UWB, RFID, and 5G technologies. Her current research interests include design methodologies, signal processing, and hardware development for telecommunication systems.



**Roc Berenguer** (M'05–SM'16) received the M.Sc. and Ph.D. degrees from TECNUN—University of Navarra, Donostia-San Sebastian, Spain, in 1996 and 2000, respectively.

From 1999 to 2015, he was with the Ceit-IK4 Research Centre, first as an Associated Researcher until 2013 and then as the Head of the Electronics and Communication Unit until 2015. Through Ceit-IK4 and INCIDE (spin-off of the Ceit's COMMIC Group), he was an External Consultant with Siemens, Munich, Germany, in 2000, Hitachi Microsystems Europe, Maidenhead, U.K., in 2001, Xignal Technologies, Munich, from 2001 to 2002, Seiko-Epson, Barcelona, Spain, from 2006 to 2007, and Innophase Inc., Chicago, IL, USA, from 2012 to 2014, where he collaborated in the design of several RF front ends for wireless standards, such as GSM-EDGE, DAB, and Wibree. He has transferred technology to two start-up companies: INCIDE S.A. in 2000 (April 2014 INCIDE was acquired by IXYS and changed its name to IXYS-San Sebastian) and FARSENS S.L. in 2008. In 2009, he was a Visiting Researcher with the Illinois Institute of Technology (IIT), Chicago, where he was involved in the design of a 77-GHz receiver front end in 65-nm CMOS for an FM-CW automotive radar. Since then, he is also an Affiliated Researcher with the High Performance Integrated Circuits and Microsystems Laboratory, IIT. During the summer semester of 2010, he was a Visiting Scholar with the High Speed Electronics Laboratory, University of California at Los Angeles (UCLA), Los Angeles, CA, USA, where he was involved in the design of a power amplifiers at 60 GHz. He is currently an Associate Professor with the Electrical, Electronic and Control Engineering Department, TECNUN—University of Navarra. He is also a Senior RFIC Design Engineer with InnoPhase Inc., San Diego, CA, USA. His technical expertise and research interests include CMOS RF and mm-wave IC design, ultralow power analog circuit design for battery-less sensor nodes, and high-speed signal processing. He has authored or coauthored more than 70 refereed publications in journals and conferences. He holds ten patents. He coauthored *Design and Test of High Quality Integrated Inductors for RF Applications in Conventional Technologies* (Springer, 2003), *GPS and Galileo: Dual RF Front-End Receiver Design, Fabrication and Test* (McGraw-Hill, 2008), and *Linear CMOS RF Power Amplifiers* (Springer, 2014).

Dr. Berenguer is an Advisor of the Spanish Agency of Evaluation and Prospective (ANEPE). He served on the Technical Program Committee of the IEEE European Solid State Circuit Conference, the IEEE Midwest Symposium Circuits and Systems, and the IEEE Ph.D. Research in Microelectronics and Electronics. He also served as a Reviewer for several journals, such as the IEEE JOURNAL OF SOLID-STATE CIRCUITS, the IEEE TRANSACTIONS ON MICROWAVE THEORY AND TECHNIQUES, the IEEE TRANSACTIONS ON CIRCUITS AND SYSTEMS—I: REGULAR PAPERS, and the IEEE TRANSACTIONS ON CIRCUITS AND SYSTEMS—II: BRIEFS.